Assessing continuum postulates in simulations of granular flow

Chris H. Rycroft [a,b,*], Ken Kamrin [c], Martin Z. Bazant [c,d]

[a] *Department of Mathematics, Lawrence Berkeley Laboratory, Berkeley, CA 94720, USA*

[b] *Department of Mathematics, University of California, Berkeley, CA 94720, USA*

[c] *Department of Mathematics, Massachusetts Institute of Technology, Cambridge, MA 02139, USA*

[d] *Physico-Chimie Théorique, Gulliver-CNRS, ESPCI, 10 rue Vauquelin, Paris 75005, France*

Abstract

Continuum mechanics relies on the fundamental notion of a mesoscopic volume "element" in which properties averaged over discrete particles obey deterministic relationships. Recent work on granular materials suggests a continuum law may be inapplicable, revealing inhomogeneities at the particle level, such as force chains and slow cage breaking. Here, we analyze large-scale three-dimensional Discrete-Element Method (DEM) simulations of different granular flows and show that an approximate "granular element" defined at the scale of observed dynamical correlations (roughly three to five particle diameters) has a reasonable continuum interpretation. By viewing all the simulations as an ensemble of granular elements which deform and move with the flow, we can track material evolution at a local level. Our results confirm some of the hypotheses of classical plasticity theory while contradicting others and suggest a subtle physical picture of granular failure, combining liquid-like dependence on deformation rate and solid-like dependence on strain. Our computational methods and results can be used to guide the development of more realistic continuum models, based on observed local relationships between average variables.

Key words: granular materials, numerical methods

* Corresponding author.

Email addresses: chr@math.berkeley.edu (Chris H. Rycroft), kenman@mit.edu (Ken Kamrin), bazant@mit.edu (Martin Z. Bazant).

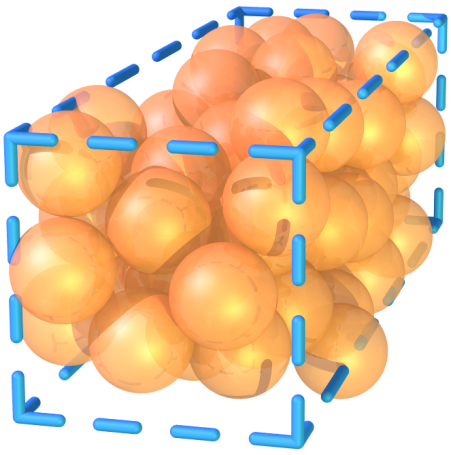

Fig. 1. A typical $2.5d \times 8d \times 2.5d$ cell of particles from a DEM simulation, which forms the basis of the approximate granular element considered in this paper.

1 Introduction

Granular materials exhibit many interesting collective phenomena and have attracted growing interest from the physics community (1; 2; 3; 4), but many of the central challenges remain unanswered. In particular, there is still no general continuum model that can describe the many phenomena of dense granular flow, such as parabolic flow (5; 6; 7) transitioning to plug flow (8) in a draining silo, wide shear zones (9) and localized shear bands (10) in Couette cells, and Bagnold scaling for inclined plane flows (11; 12). This is in contrast to the hydrodynamics of dilute granular materials and molecular fluids, for which accurate continuum models can be systematically derived by averaging over particle collisions in an idealized element (13).

Recent work has revealed microscopic features of dense granular materials, which seem to defy a simple continuum description. These include: (i) complex, fractal networks of force chains, which are inhomogeneous down to the particle level (14; 15; 16; 17; 18; 19; 20; 21); (ii) anomalous, non-collisional particle dynamics with very slow cage breaking (7; 22; 23); (iii) proximity to the jamming transition, where geometrical packing constraints suppress any dynamics (24; 25); (iv) a lack of thermal equilibrium in the conventional sense, since particles only move in response to external forces, motivating new definitions of temperature (26; 27; 28; 29); and (v) a wide range of dynamical response, from liquid-like to solid-like (2; 30; 31). The first four points cast serious doubt on the prospects of a continuum law. The fifth means that the full stress tensor must be described, and it may depend on strain, deformation rate, and material variables that can evolve during the process.

We thus arrive at the fundamental question: can a "granular element" be meaningfully defined, and if so, what is its rheology? The oldest definition

corresponds to the two-dimensional "Ideal Coulomb Material", in which the granular element behaves like a rigid solid, which undergoes failure if the ratio of shear stress to normal stress on any plane exceeds a critical value μ, the Coulomb internal friction coefficient (32). The stress tensor is determined by mechanical equilibrium along with the hypothesis of *incipient yield*, which asserts that the yield criterion is attained everywhere at all times (in a "limit-state"). In limit-state Mohr–Coulomb plasticity, these conditions are assumed to hold even if boundary conditions allow for plastic yielding. In that case, the velocity follows from the assumption of *coaxiality*, which asserts that the stress and deformation rate have the same eigendirections. The resulting equations of limit-state Mohr–Coulomb plasticity have been used extensively in engineering applications (32; 33), but their general solution requires sophisticated numerical techniques to capture shock-like discontinuities in stress and velocity, which arise even in relatively simple geometries (34; 35; 36). Besides the questionable physical basis of such discontinuities, the model is incapable of describing most of the flows listed above, even qualitatively.

Recently, a number of theories have been developed to more precisely capture the underlying physics of a granular element. The Shear Transformation Zone theory et al. (37; 38) provides a mechanism for the element to retain a memory of its shearing history, through an auxiliary continuum variable, the STZ density. The partial fluidization model of Aranson and Tsimring (30; 31) introduces another auxiliary "order parameter" for the granular element, which controls the size of the viscous-like contribution to the stress tensor. From extensive experimental studies of inclined-plane flows, Jop et al. have proposed a 3D flow rule for a granular element at yield (39). Although each of these models has had successes, none constitutes a complete continuum description of granular flow, which can be applied to more than one of the geometries listed above under arbitrary traction/kinematic boundary conditions.

Our group has developed a different, multiscale theoretical framework (22; 23; 40; 41), that was initially motivated by the search for a mechanism to describe microscopic particle motion and rearrangement within a granular flow. Granular materials form amorphous random packings, and an individual particle within this structure typically cannot move by itself, as it is strongly geometrically constrained by its neighbors; in order for flow to occur, particle motion must take place co-operatively. This led to the postulation of a *spot* (22) that would mediate a correlated motion of particles on a mesoscopic scale. The diameter of a spot can be inferred from tracer-diffusion measurements in silo drainage (7; 42), and typically our group has found a scale on the order of three to five particle diameters. Independently, the same length scale also emerges from direct measurements of spatial velocity correlations in drainage experiments (43) and DEM simulations (23). Using this scale in spot-based drainage simulations also produces incredibly realistic flowing random packings (23). These ideas have also been incorporated into a general

theory, which can predict a variety of experimental flow profiles, again using the same length scale (and no other fitting parameters) (40). Assuming stresses at incipient yield, the coaxial flow rule is replaced by a "stochastic flow rule" (SFR) in which spots of mobilized material perform random walks along slip lines, biased by local stress imbalances. The resulting theory is the first to predict both gravity-driven flow in a silo and shear flow in a Couette cell (40; 41), so a major motivation for this work is to directly test its basic assumptions.

This prompts us to study rheological properties of granular media over volume elements of size comparable to the width of dynamical correlations, $3d$ to $5d$. By "element", we are referring to an approximate Representative Volume Element (RVE) (44). A uniform stress state expressed at the boundaries of an RVE should couple to a predictable homogeneous boundary deformation. But to be technically precise, full determinism of this coupling is deducible only for an element containing infinitely many microconstituents, so that average behavior over all microevents approaches a Dirac-delta function about the mean. Realistically, all materials possess a finite micro-length, so any RVE behavior must be interpreted within some acceptable noise tolerance. Hierarchical relationships for such noise bounds have been deduced by Ostoja-Starzewski (45) in terms of the ratio $\delta = L_{\text{meso}}/L_{\text{micro}}$, where averaging is over random realizations of a heterogeneous continuum material. For finite δ, the element is more aptly referred to as a Statistical Volume Element (SVE), which approaches RVE in the limit $\delta \to \infty$. While we use the term RVE throughout this work, in some sense we mean a granular SVE with some acceptably small, and quantifiable, level of noise. However, we stress that randomness in our simulations comes from packing constraints and discrete rearrangements of a homogeneous model material consisting of frictional, viscoelastic spheres; as in molecular materials which are routinely described by continuum mechanics, we will show that meaningful continuum averages, satisfying predictable relations with controlled fluctuations, can be defined at the scale of observed dynamical correlations.

The RVE must be small compared to the macroscopic length of the flow, allowing the granular domain to deform as a network of RVEs, each one experiencing close to uniform boundary conditions. If gradients in the stress or deformation fields become too sharp, the noise in the element response must inevitably increase. This may pose an issue for materials that can form shear bands. Granular media are known to exhibit shear-banding phenomena in certain circumstances, though it should be noted that 3D bands tend to have a width of $10d$ to $15d$ (46), suggesting a $3d$ to $5d$ wide element may still suffice. This also supports our major belief that unless conditions are exotic enough to change the dynamical correlation length (e.g. large applied gradients in loading or shear), an element at this $3d$ to $5d$ length scale should be small enough to describe a "standard" set of dense flows.

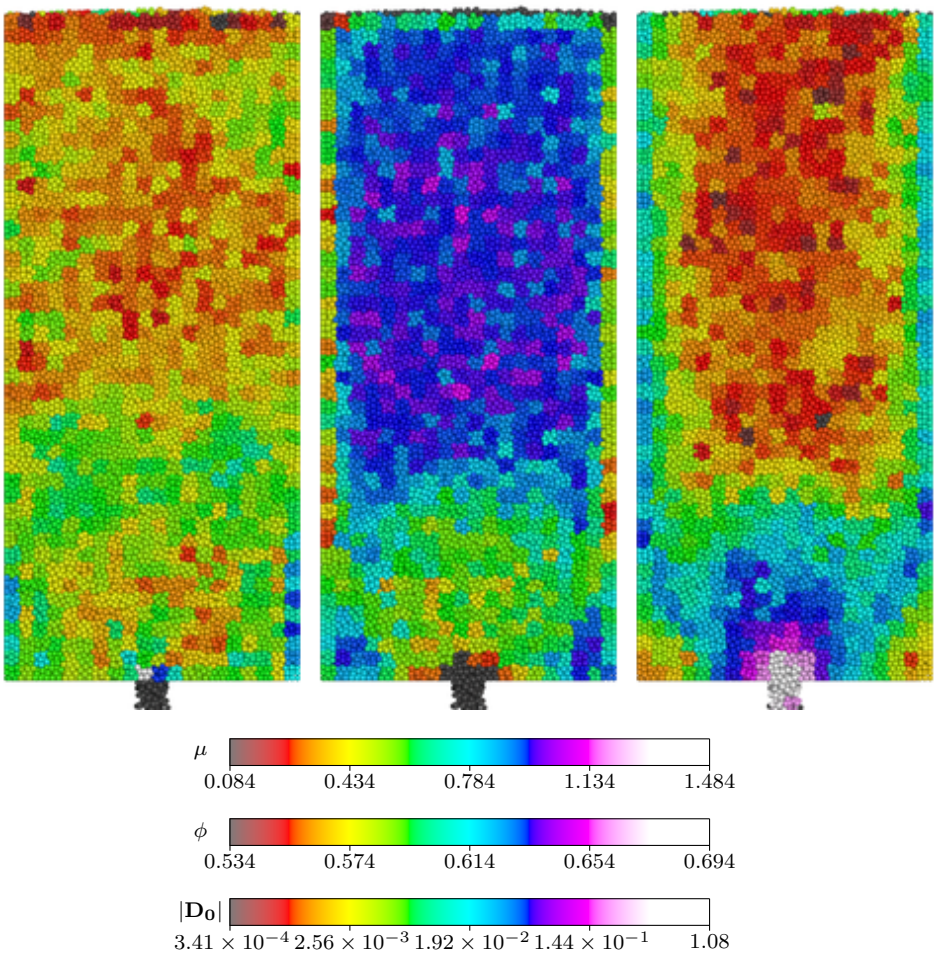

Fig. 2. Three computed material quantities (μ, left; packing fraction ϕ, center; magnitude of deviatoric deformation rate $|\mathbf{D_0}|$, right) in the tall silo drainage simulation, shown at $t = 25\tau$. All the particles in each computational cell are colored according to the computed material variables for that cell. μ and ϕ are dimensionless, while $|\mathbf{D_0}|$ has units of τ^{-1}. A movie of this simulation is available in the supplementary information.

Although this scale may seem somewhat arbitrary, its validity could be verified by systematic coarse graining procedures, such as those used by Goldenberg et al. to construct continuum elasticity at a given length scale (47) from discrete simulations of granular materials (19; 20; 21), but it is beyond the scope of this work to extend such methods to situations of plastic flow. Instead, we fix a length scale for the RVE, motivated by dynamical correlations observed in the same model material, and focus on testing relationships between a variety of continuum variables at that particular scale.

2 Methods

In this paper, we present the results of several large-scale DEM simulations carried out using the Large-scale Atomic/Molecular Massively Parallel Simulator (LAMMPS) developed by Sandia National Laboratories (48). The contact model is based on that developed by Cundall and Strack (49), and has been well-tested and used in many other studies (50; 11; 51; 52). In the simulations, frictional particles of mass m and diameter d experience gravity g in the negative z direction, which can be used to define a natural time unit $\tau = \sqrt{d/g}$. For the simulations considered here, we restrict attention to cases which are periodic in the horizontal y direction with period $8d$, although this still allows us to consider fully three-dimensional stresses.

Particles interact according to Hookean, history dependent contact forces. If a particle and its neighbor have a separation vector $\mathbf{r}$, and the two particles are in contact, so that $\delta = d - |\mathbf{r}| > 0$, then they experience a force $\mathbf{F} = \mathbf{F}_n + \mathbf{F}_t$, where the normal and tangential components are given by

$$\mathbf{F}_n = \left(k_n \delta \mathbf{n} - \frac{\gamma_n \mathbf{v}_n}{2} \right)$$
$$\mathbf{F}_t = \left(-k_t \Delta \mathbf{s}_t - \frac{\gamma_t \mathbf{v}_t}{2} \right).$$

Here, $\mathbf{n} = \mathbf{r}/|\mathbf{r}|$. $\mathbf{v}_n$ and $\mathbf{v}_t$ are the normal and tangential components of the relative surface velocity, and $k_{n,t}$ and $\gamma_{n,t}$ are the elastic and viscoelastic constants, respectively. $\Delta \mathbf{s}_t$ is the elastic tangential displacement between spheres, obtained by integrating tangential relative velocities during elastic deformation for the lifetime of the contact, and is truncated as necessary to satisfy a local Coulomb yield criterion $|\mathbf{F}_t| \leq \mu_f |\mathbf{F}_n|$. Particle–wall interactions are treated identically, but the particle–wall friction coefficient is set independently. For the current simulations we set $k_t = \frac{2}{7} k_n$, and choose $k_n = 2 \times 10^5 mg/d$. While this is significantly less than would be realistic for glass spheres, where we expect $k_n \sim 10^{10} mg/d$, such a spring constant would be prohibitively computationally expensive, as the time step must have the form $\delta t \propto k_n^{-1/2}$ for collisions to be modeled effectively. Previous simulations have shown that increasing k_n does not significantly alter physical results (50). We make use of a time step of $\delta t = 10^{-4} \tau$, and damping coefficients $\gamma_n = \gamma_t = 50\sqrt{g/d}$.

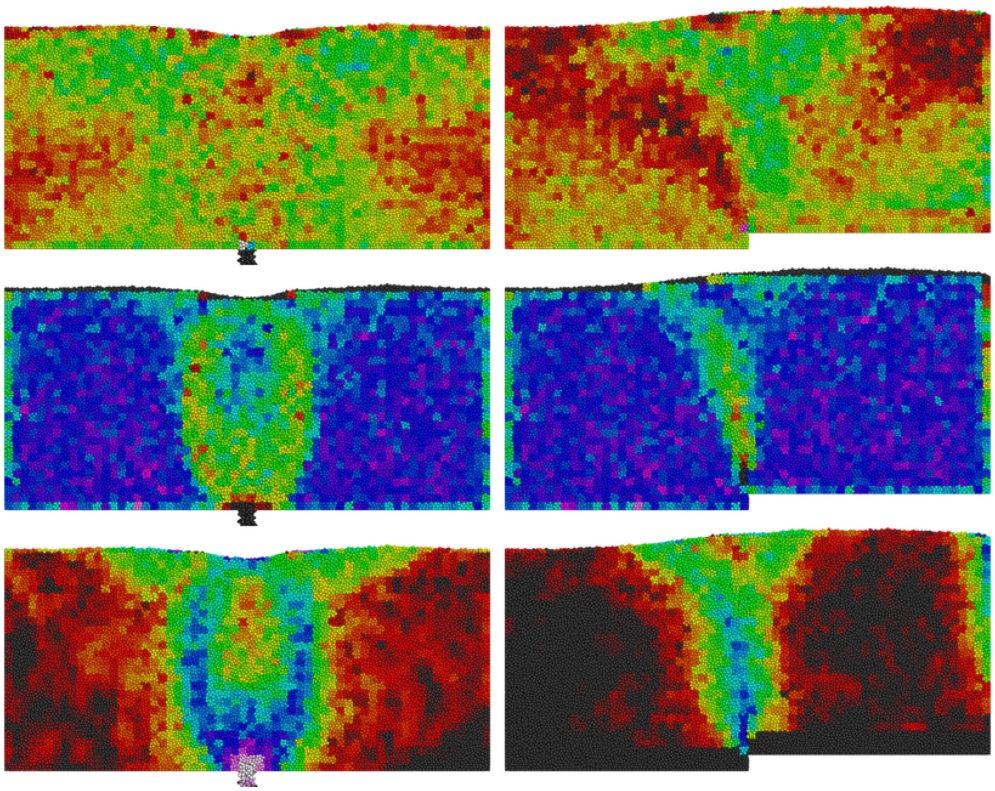

Fig. 3. Three computed material quantities (μ, top; packing fraction ϕ, middle; magnitude of deviatoric deformation rate $|\mathbf{D_0}|$, bottom) in the wide silo for the drainage simulation at $t = 40\tau$ (left) and the pushing simulation at $t = 25\tau$ (right). The color scheme used is the same as that in Figure 2. Movies of these two simulations are available in the supplementary information.

3 Computation of material variables

Since our overall aim is to extract information about the inherent properties of a granular material, and not its behavior in a particular situation, we consider a variety of granular flows in different geometries. We consider a tall silo with base at $z = 0$ and walls at $x = \pm 25d$, and create an initial packing by pouring in 55000 particles from $z = 160d$ at a constant rate of $123\tau^{-1}$ to fill the silo to an approximate height of $z = 114d$. We also consider a wide silo, with a base at $z = 0$ and walls at $x \pm 75d$, and pour in 100000 particles from $z = 160d$ at a constant rate of $379\tau^{-1}$, to fill the silo to a height of approximately $z = 69d$. For both situations, the initial packing fraction is approximately 63.5%.

For both packings, a drainage simulation is then carried out, by opening a $6d$-wide slit in the center of the container base. In addition, a pushing simulation is carried out in the wide silo, by freezing all particles whose centers initially satisfy $z < 7.5d$, and then moving those with $x > 0$ upwards at a constant speed of $0.2d\tau^{-1}$. All three of these simulations are quite different in form. The tall silo drainage simulation is different from the wide silo since the velocity

profile is strongly affected by the presence of the vertical walls. The pushing simulation corresponds to an active forcing of the material, while the drainage simulations are generated by a passive response to gravity.

For each simulation, a snapshot of all particle positions is recorded at fixed intervals of 0.2τ. In addition to this information, numerous material quantities are calculated in a grid of cells of size $2.5d \times 8d \times 2.5d$, at the scale of the granular element. The local packing fraction ϕ is computed in each cell of interest by evaluating the precise fraction of the cuboidal cell volume which is occupied by the particles. The stress tensor in each cell is calculated by looking at the forces between particles on contact. If there are N particles in the cell, and particle l has a total of N_l contacts, then an approximate stress tensor can be defined as in (53) and simplified for spherical grains to give

$$T_{ij} = \frac{1}{V} \sum_{l=1}^{N} \sum_{k=1}^{N_l} \Delta x_i^{(k,l)} F_j^{(k,l)}$$

where $\mathbf{F}^{(k,l)}$ is the force of the kth contact on particle l, and $\mathbf{\Delta x}^{(k,l)}$ is the separation vector from the center of particle l to its kth contact.

From this, we can define a pressure $p = -\frac{1}{3} \operatorname{tr} \mathbf{T}$ and a deviatoric stress tensor $\mathbf{T_0} = \mathbf{T} + \frac{1}{3} p \mathbf{1}$. To calculate the value of μ, we make use of the classical Mohr–Coulomb definition, in which μ is the ratio of shear stress to normal stress acting on an internal plane of the material element maximized over all possible internal planes. Algebraically, if $\mathbf{T}$ has eigenvalues $\lambda_1 < \lambda_2 < \lambda_3$, then

$$\mu = \frac{\lambda_3 - \lambda_1}{\lambda_3 + \lambda_1}.$$

We also considered the alternative Drucker–Prager definition of the yield parameter (54), which is defined as the ratio of the pressure p to the equivalent shear stress $|\mathbf{T_0}|/\sqrt{2}$, so that $\mu_{\mathrm{DP}} = |\mathbf{T_0}|/p\sqrt{2}$. A plot of μ against μ_{DP} using data from the three simulations appears linear, with a correlation coefficient of 0.96. Due to this high level of agreement in all our simulations, we present results using the Mohr–Coulomb definition only, and we leave an in-depth study of the different definitions for later work. Since the Drucker–Prager definition includes a dependence on the intermediate stress eigenvalue λ_2, the differences between the μ_{DP} and the Mohr–Coulomb μ may be more apparent in non-periodic, fully three-dimensional situations, which are beyond the scope of this paper.

To calculate the velocity gradient $\mathbf{L}$ in a cell, we consider the least squares regression problem

$$\mathbf{v} = \mathbf{L}\mathbf{x} + \mathbf{v}^0.$$

Here $\mathbf{x}$ and $\mathbf{v}$ are the instantaneous positions and velocities of all particles within the cell. The average cell velocity $\mathbf{v}^0$ and the velocity gradient are

found by minimizing the sum of squares of residuals. The deformation rate tensor [1] is then defined as the symmetric part of $\mathbf{L}$, namely

$$\mathbf{D} = \frac{\mathbf{L} + \mathbf{L}^{\mathrm{T}}}{2}.$$

From this, the deviatoric deformation rate tensor is defined as $\mathbf{D_0} = \mathbf{D} - \frac{1}{3}(\operatorname{tr}\mathbf{D})\mathbf{1}$. In most cases we expect $\mathbf{D_0} \approx \mathbf{D}$ since the density of the granular material does not fluctuate by a large amount, making the contribution to $\mathbf{D}$ from shearing larger than that from dilation. For some of the analysis, we made use of a normalized deformation rate $|\mathbf{I_0}| = |\mathbf{D_0}|d\sqrt{\rho_s/p}$ where ρ_s is the particle density; this has been studied by others (39; 55; 56) and is well-suited for use in rate sensitive granular constitutive laws.

It is possible that the instantaneous velocities used in the computation of $\mathbf{D}$ may be subject to simulation artefacts, such as particle rattling, or elastic behavior arising from the spring–dashpot contact model. We therefore carried out the same analysis based on velocities computed by interpolating particle positions between successive snapshots, effectively giving an averaged velocity on a scale of 0.2τ, an order of magnitude larger than the timescale of a typical particle–particle interaction. A plot of $\log|\mathbf{D_0}|$ for the two different computation methods appears linear, with a correlation coefficient of 0.98. Due to the high level agreement, all our results are presented using the instantaneous velocities in the deformation rate calculation.

4 Stress, deformation rate, and packing fraction

Figure 2 shows plots of μ, ϕ, and $|\mathbf{D_0}|$ for the tall silo drainage simulation. Near the orifice, there is a converging region of flow, that has roughly parabolic streamlines. Higher in the container, there is a transition to uniform flow, where the particles drop like a plug, behave like a solid, and experience little rearrangement, as has been seen in similar situations (8). The plot of $|\mathbf{D_0}|$ supports these results. High in the container, very little rearrangement is seen, while there is a sharp transition to high values when the packing must undergo deformation to pass through the orifice.

It is clear from the plots that ϕ and $|\mathbf{D_0}|$ are closely correlated. In the upper region, where particles are falling like a plug, the packing fraction remains constant. In the converging region, the packing fraction decreases, as the particles must have more free space in order to geometrically rearrange; this is studied quantitatively later.

[1] This tensor is sometimes called the "strain rate", but for large deformations this is misleading since it is not the rate-of-change of any finite strain tensor.

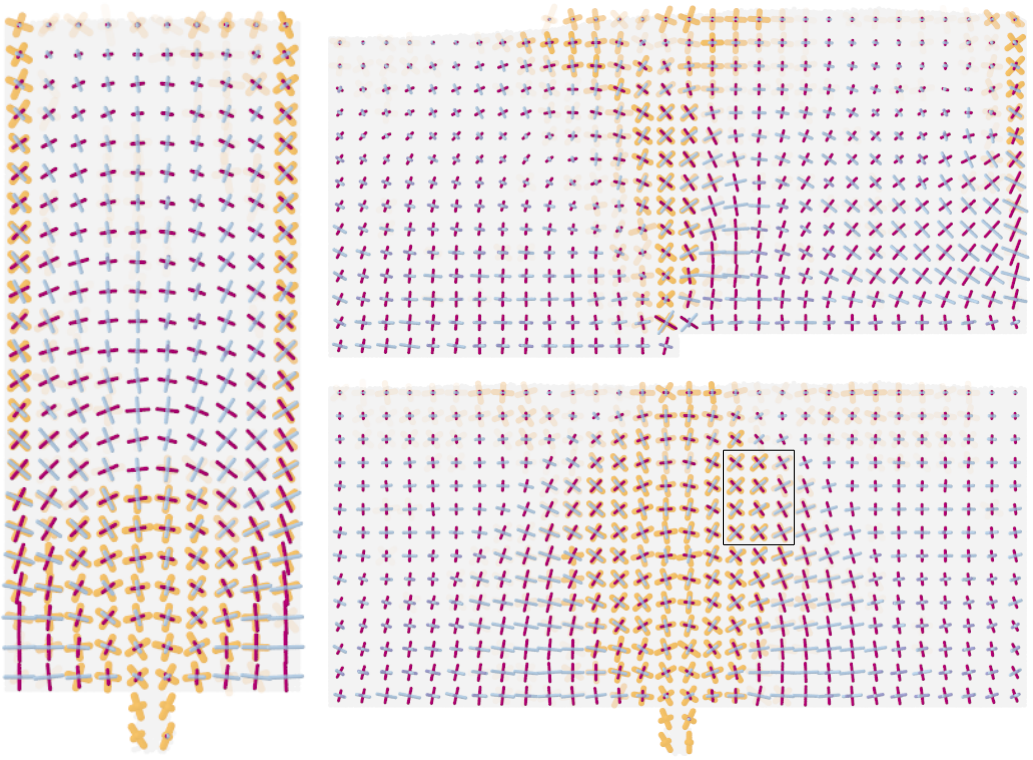

Fig. 4. Plots of the directions and magnitudes of the eigenvectors of the deviatoric stress and deformation rate tensors, calculated instantaneously in $5d \times 8d \times 5d$ boxes with no time-averaging. The maximal stress eigenvector is shown in purple, with the other two eigenvectors being shown in blue. In the regions where deformation is occurring, the maximal and minimal eigenvectors of the deformation rate tensors are plotted in orange. In all cases, a high degree of alignment between the two tensors can be seen. Additional plots are available in the supplementary information.

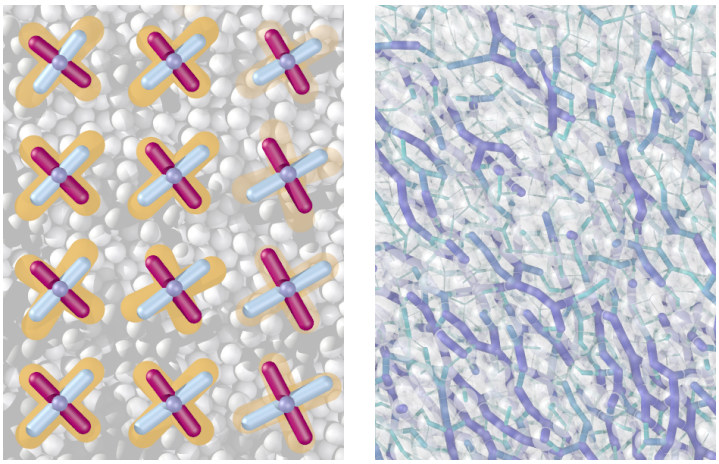

Fig. 5. Left: A detail of the computed stresses and deformation rates for region enclosed by the black rectangle in Figure 4. Right: the individual forces in the same region.

Of the three plots, μ exhibits the largest fluctuations, which we attribute to the fact that it is a ratio between two computed quantities. However, large variations over the range 0.2 to 0.6 can be clearly seen. This immediately calls the Mohr–Coulomb incipient yield hypothesis into question, which would predict that μ would be constant everywhere. At first sight, the spatial differences in μ appear not directly correlated with the other two. However, regions of higher μ exist at the interface between the plug-like region, and the converging flow region; this will be expanded on later. Figure 3 shows the same three plots for the wide drainage and wide pushing simulations, and the same relationships between the three quantities can be observed.

Figure 4 shows the directions and magnitudes of the eigenvectors of the deviatoric stress tensor for three different situations. For these images, the stress tensor was calculated on a $5d \times 8d \times 5d$ grid, by averaging the computed stress tensor in 2×2 blocks of cells. Even though they were computed using local, instantaneous data, we can see that in all situations, the stress tensors are smooth, and exhibit none of the shocks predicted by limit-state plasticity theory. For regions undergoing deformation, the eigenvectors of $\mathbf{D_0}$ are also shown in Figure 4. We see that in all areas where there is appreciable deformation rate, there is a strong alignment between the two sets of eigenvectors, which is surprising given that the individual forces, as shown for a small region in Figure 5, exhibit large inhomogeneities.

For the plots of Figure 4, the average angular differential between the maximal eigenvectors is approximately 12°. If the plots are time-averaged over a window of twenty frames, then the mean angular differential drops to 6.7°. Averaging over progressively larger time windows also allows us to verify coaxiality as far into the granular packing as one can reasonably define a deformation rate tensor. Coaxiality is a consequence of material isotropy at the scale of a continuum element, so it appears that increasing the time window increases the extent to which the liquid-like material flows like a true continuous fluid.

In light of the successes of the SFR (40; 41) it is interesting to note that our results are the opposite to its hypotheses: incipient Mohr–Coulomb yield does not hold, while coaxiality does, especially over longer time scales in the flowing region. In may be that the basic SFR concept of random spot-based propagation of fluidization holds at small time scales, only with different stress models or spot dynamics. However, our results constrain any statistical theory to uphold coaxiality after time averaging, and even instantaneously to some degree in steady flows. On the other hand, the data does not rule out departures from coaxiality in regions of very slow or intermittent flow at the onset of yielding, where the arguments behind the SFR should have the most validity.

Using this data, we tested the codirectionality hypothesis $\mathbf{T_0} \propto \mathbf{D_0}$. This assertion is stronger than just coaxiality and has been presumed by some (39)

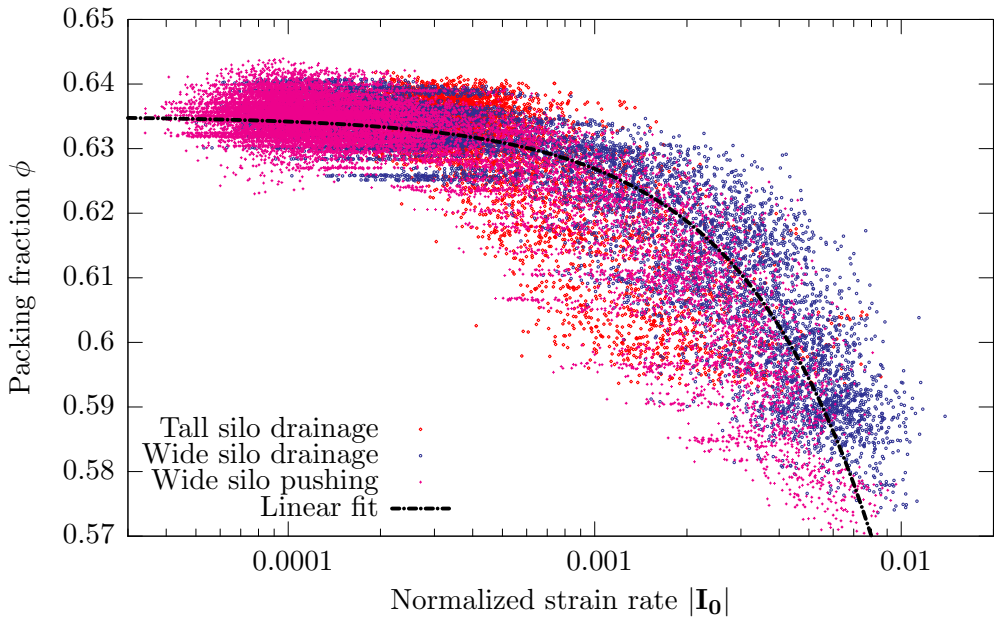

Fig. 6. A plot of packing fraction ϕ versus normalized deformation rate $|\mathbf{I_0}|$. Each point corresponds to the computed material quantities for a granular element from one of the three DEM simulations.

while challenged by others (57). Our data reveals reasonably large variations from purely codirectional flow. It is possible that double-shearing (58) may be a more appropriate hypothesis, but more testing is necessary.

5 Evolution of material variables

We now investigate quantitatively the connections seen above, by viewing all the material cells from the different simulations as an ensemble of approximate "granular elements", and seeking statistical relationships between them. As a first example, consider Figure 6, showing a plot of $|\mathbf{I_0}|$ against ϕ. Each point on the graph corresponds to the instantaneous computed values of a material element from one of the simulations, during a period when steady flow has developed. We see an approximate collapse of the points from the three simulations, suggesting that the correlation we are viewing is a property inherent to the granular material, and not tied to any particular simulation configuration. Also shown is a fit line $|\mathbf{I_0}| = 0.123(0.635 - \phi)$, The linear relationship is consistent with the two-dimensional results of da Cruz (55).

While instructive, the above approach will only allow us to search for direct correlations between variables. In reality, we expect that these are related in a more complicated way, and that differential relationships may exist; there may also be internal state variables which we are not measuring, that relate to an element's history of deformation and stress. Because of these complications,

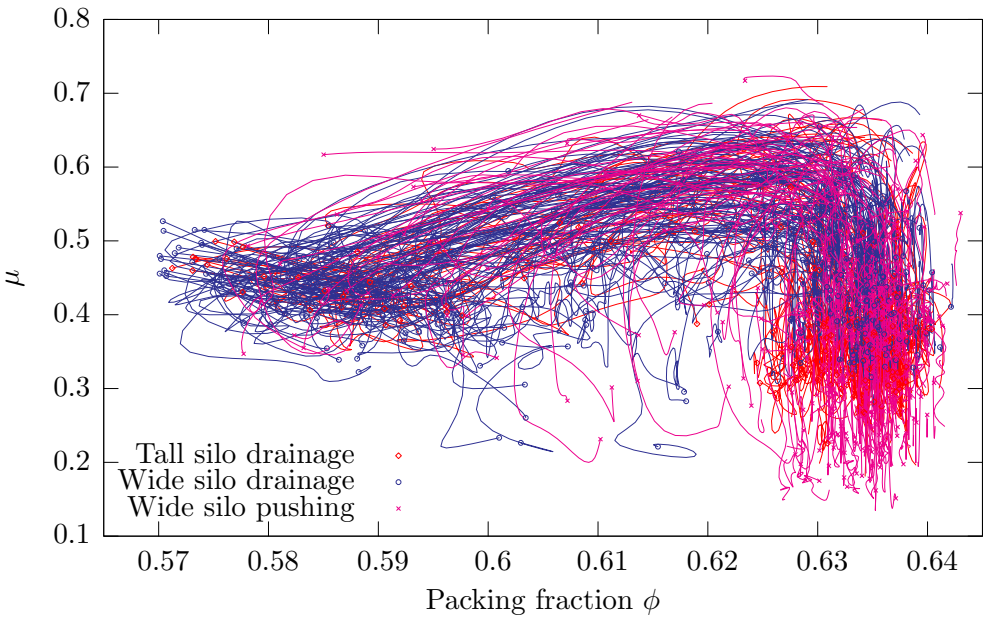

Fig. 7. Lagrangian tracer plot of μ versus packing fraction ϕ. Each line corresponds to the trace in phase space of a granular element in one of the three simulations.

it is natural to switch from an Eulerian to Lagrangian approach: rather than viewing our data set as an ensemble over fixed spatial positions, we treat it as an ensemble of material elements which deform and move with the flow. Each granular element corresponds to an approximate trace in the phase space of material variables over its history during the simulation.

To correctly implement this, we must also take into account that a granular cell may move during the simulation. We therefore initially introduced a number of tracer positions on a $5d \times 5d$ lattice. During the simulation, the tracer positions are advected according the average background velocity of the particles. For each tracer, a history of a granular element is created by linearly interpolating all the material variables from the underlying raw simulation data on the $2.5d \times 2.5d$ lattice.

Figure 7 shows material tracers in a plot of μ versus ϕ for the three different simulations. The plot shows us that, while μ is not directly correlated to ϕ, it plays an important role in the failure of a granular element. The majority of tracers start off on the right side of the graph, at the initial packing fraction of 63.5%. Those tracers corresponding to failing elements take a path in an inverted U-shape, first attaining a value of μ of approximately 0.6 before starting to decrease in packing fraction. A material element will dilate only if a critical value of μ is first attained. This directly relates to the behavior seen in Figures 2 and 3, where it was noted that areas of larger μ were located at the interface between solid-like and liquid-like regions. Also visible in 7 is a tendency for dilated elements which experience a low value of μ to recompact slightly.

Some of these results are in agreement with past granular plasticity models. In Critical State Soil Mechanics (CSSM) (59), an initially overconsolidated material at a fixed confining pressure p undergoes a decrease in both μ and packing fraction ϕ upon plastic failure by shearing. After sufficient shearing, ϕ approaches a constant-volume value that depends solely on the confining pressure, and μ approaches a material constant μ_{CV}. The left-hand side of Figure 7 displays a similar decrease in μ over decreasing ϕ, and the paths of Lagrangian tracers appear to approach a roughly constant μ. However, it is difficult to discern from this conglomerated data whether the final μ state is truly constant, or if the spread in final packing fraction could be accounted for solely by pressure variations among trajectories. Homogeneous shear tests, which are outside our current interest, are clearly better-suited for expounding these particular behaviors. Turning attention to the right-hand side of Figure 7, the initial upshoot in μ to its peak value appears to happen over a relatively small change in ϕ. It is not at the moment clear whether this $\Delta\phi$ accounts solely for elastic mechanisms (as in the Cam–Clay and Modified Cam–Clay models of CSSM), or whether some plastic evolution of μ also takes place in this zone (as per the Anand–Gu model (60)). But despite these details, we are content that the general trend displayed in Figure 7 is in concert with past theoretical development from the plasticity vantagepoint.

The Lagrangian approach also allows us to get a clearer insight into shear dilation, the precise mechanics of which remains an open study. Our results show correlations between packing fraction and deformation rate, in agreement with other authors. However, several models for granular plasticity presume "rate-independence", which asserts that dilation evolves with total plastic strain (59; 61; 60). These models are typically used under quasi-static flow conditions, where the effect of shear-rate should be minimal. Since one would expect for a single snapshot, the regions of high strain could roughly be correlated with the regions of high deformation rate, we defer to a quantitative analysis for improved resolution of this interdependence.

Strain is calculated from the simulation data by using the snapshots of all particle positions. At $t = 0$, a $5d \times 8d \times 5d$ box of particles is labeled, centered on each material tracer. Let $\mathbf{x}^i$ be the initial particle positions in a particular box. A deformation gradient tensor $\mathbf{F}$ and an overall translation $\mathbf{x}^0$ can then be found by solving the least squares regression problem

$$\mathbf{x} = \mathbf{F}\mathbf{x}^i + \mathbf{x}^0$$

where $\mathbf{x}$ are the current particle positions. We then compute the polar decomposition $\mathbf{F} = \mathbf{R}\mathbf{U}$ where $\mathbf{R}$ is a rotation matrix, and the stretch $\mathbf{U}$ is a symmetric positive definite matrix. Unlike infinitessimal theory, there are many valid ways to define the strain tensor for large deformations, though each way must be a function of $\mathbf{U}$ which asymptotes under small stretches

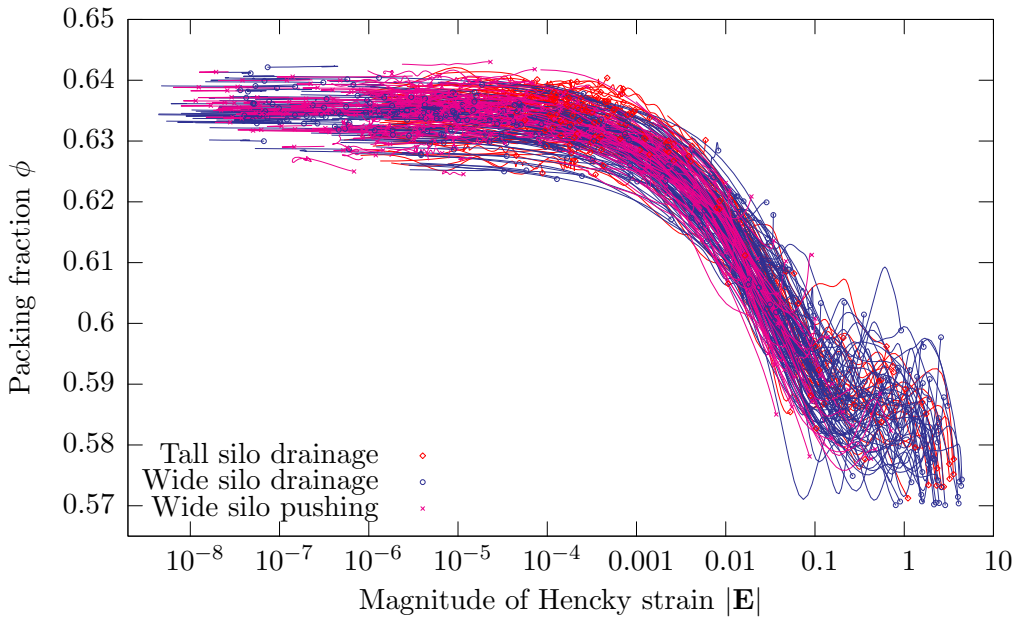

Fig. 8. Lagrangian tracer plot of packing fraction ϕ versus magnitude of Hencky strain $|\mathbf{E}|$.

to the well-known infinitessimal definition. Here, we choose the Hencky strain measure $\mathbf{E} \equiv \log \mathbf{U}$, which has the additional property that strains are additive in the absence of rotation.

Figure 8 shows a plot of packing fraction versus strain, with a sharp collapse of the trajectories across several simulations. In order to be consistent with Figure 6, strain must be instrumental in the process by which the material dilates, but deformation rate sets the final packing fraction.

6 Conclusion

The results show that it is possible to make a direct connection between continuum theories and particle-based simulations of dense granular flow at the local level. We have demonstrated that in three dimensions, an approximate granular element defined at the scale of the dynamical correlations exhibits a small enough amount of statistical noise to make many inferences about the rheology of granular materials. Consistent with the results of da Cruz et al. (55) and Lois et al. (56), we have shown a direct link between normalized deformation rate and packing fraction and, in agreement with (55), have observed that this relationship is approximately linear. However, while previous work was carried out in 2D, we have shown this result locally in 3D using multiple geometries with far less symmetry. Our results also show that while deformation rate is important in determining the steady state which a packing

will reach, the total strain plays an important role in determining the transient process by which the deformation takes place. Together these results suggest a complex picture of granular failure, suggesting that a continuum model should incorporate both deformation rate and total deformation.

The numerical techniques presented here have several advantages over more traditional approaches, such as simulations within a periodic cell. Our approach allows for continuum hypotheses to be evaluated locally and instantaneously within the context of real flows. By breaking up several different simulations into a large ensemble of granular elements we are able to test continuum hypotheses across a wide variety of potential configurations, giving us more confidence that the properties we observe are inherent in the material, and not tied to one particular situation. By making use of a Lagrangian perspective, and tracing elements with the flow, we are able to search for more complex differential relationships. These techniques could easily be extended to other situations, and in the future we hope to directly evaluate the some of the recently proposed theories for granular materials (40; 39; 30; 37). These are frequently characterized by having a microscopic continuum quantity, such as STZ populations $n_{\pm}$, SFR spot density ρ_s, or partial fluidization parameter ρ, and part of the challenge in investigating these quantities will be to understand how they directly relate to the microscopic packing structure. Another promising avenue to pursue is to better understand the role of total strain. While strain appeared to play a crucial role in interpreting our data, it is an undesirable quantity to use in an eventual continuum theory of granular materials, since it is always tied to an initial reference state. Examining fully three-dimensional situations may also provide useful clues, since it would provide greater variation in the stress tensor, allowing for an in-depth analysis of the relative merits of the different proposed granular yield criteria and the role, if any, played by the intermediate stress eigenvalue, a question which is currently unresolved.

References

[1] H. M. Jaeger, S. R. Nagel, Physics of the granular state, Science 255 (1992) 1523–1531.

[2] H. M. Jaeger, S. R. Nagel, R. P. Behringer, Granular solids, liquids, and gases, Rev. Mod. Phys. 68 (1996) 1259–1273.

[3] P. G. de Gennes, Granular matter: a tentative view, Rev. Mod. Phys. 71 (1999) S374–S382.

[4] T. Halsey, A. Mehta (Eds.), Challenges in Granular Physics, World Scientific, 2002.

[5] A. Medina, J. A. Cordova, E. Luna, C. Trevino, Velocity field measure-

ments in granular gravity flow in a near 2D silo, Physics Letters A 220 (1998) 111–116.
[6] R. M. Nedderman, U. Tüzün, Kinematic model for the flow of granular materials, Powder Technology 22 (1979) 243.
[7] J. Choi, A. Kudrolli, R. R. Rosales, M. Z. Bazant, Diffusion and mixing in gravity driven dense granular flows, Phys. Rev. Lett. 92 (2004) 174301.
[8] C. H. Rycroft, G. S. Grest, J. W. Landry, M. Z. Bazant, Analysis of granular flow in a pebble-bed nuclear reactor, Phys. Rev. E 74 (2006) 021306.
[9] D. Fenistein, M. van Hecke, Wide shear zones in granular bulk flow, Nature 425 (2003) 256.
[10] D. M. Mueth, Measurements of particle dynamics in slow, dense granular couette flow, Phys. Rev. E. 67 (2003) 011304.
[11] L. E. Silbert, D. Ertaş, G. S. Grest, T. C. Halsey, D. Levine, S. J. Plimpton, Granular flow down an inclined plane: Bagnold scaling and rheology, Phys. Rev. E 64 (5) (2001) 051302.
[12] O. Pouliquen, Scaling laws in granular flows down rough inclined planes, Phys. Fluids 11 (1999) 542.
[13] J. T. Jenkins, S. B. Savage, A theory for the rapid flow of identical, smooth, nearly elastic particles, J. Fluid Mech. 130 (1983) 187–202.
[14] D. M. Mueth, H. M. Jaeger, S. R. Nagel, Force distribution in a granular medium, Phys. Rev. E 57 (1998) 3164–3169.
[15] D. L. Blair, N. Mueggenburg, A. M. Marshall, H. M. Jaeger, S. R. Nagel, Force distributions in three-dimensional granular assemblies: Effects of packing order and interparticle friction, Phys. Rev. E 63 (2001) 041304.
[16] S. F. Edwards, The equations of stress in a granular material, Physica A 249 (1998) 226–231.
[17] C. h. Liu, S. R. Nagel, D. A. Schecter, N. Coppersmith, S. Majumdar, O. Narayan, T. A. Witten, Force fluctuations in bead packs, Science 269 (1995) 513–515.
[18] T. S. Majumdar, R. P. Behringer, Contact force measurements and stress-induced anisotropy in granular materials, Nature 435 (2005) 1079–1082.
[19] C. Goldenberg, I. Goldhirsch, Force chains, microelasticity and macroelasticity, Phys. Rev. Lett. 89 (2002) 084302.
[20] C. Goldenberg, I. Goldhirsch, Small and large scale granular statics, Granular Matter 6 (2004) 87.
[21] C. Goldenberg, A. P. F. Atman, P. Claudin, G. Combe, I. Goldhirsch, Scale separation in granular packings: stress plateaus and fluctuations, Phys. Rev. Lett. 96 (2006) 168001.
[22] M. Z. Bazant, The spot model for random-packing dynamics, Mechanics of Materials 38 (2006) 717–731.
[23] C. H. Rycroft, M. Z. Bazant, G. S. Grest, J. W. Landry, Dynamics of random packings in granular flow, Phys. Rev. E 73 (2006) 051306.
[24] C. S. O'Hern, L. E. Silbert, A. J. Liu, S. R. Nagel, Jamming at zero temperature and zero applied stress: The epitome of disorder, Phys. Rev.

E 68 (2003) 011306.
[25] A. Donev, S. Torquato, F. H. Stillinger, R. Connelly, Jamming in hard sphere and disk packings, J. Appl. Phys. 95 (2004) 989–999.
[26] S. Henkes, C. S. O'hern, B. Chakraborty, Entropy and temperature of a static granular assembly: An ab initio approach, Phys. Rev. Lett. 99 (2007) 038002.
[27] S. F. Edwards, D. V. Grinev, Statistical mechanics of vibration-induced compation of powders, Phys. Rev. E 58 (1998) 4758–4762.
[28] H. A. Makse, J. Kurchan, Testing the thermodynamic approach to granular matter with a numerical model of a decisive experiment, Nature 415 (2002) 614–616.
[29] D. Serero, C. Goldenberg, S. H. Noskowicz, I. Goldhirsch, The classical granular temperature and slightly beyond, Powder Technol.
[30] I. S. Aranson, L. S. Tsimring, Continuum description of avalanches in granular media, Phys. Rev. E 64 (2001) 020301.
[31] I. S. Aranson, L. S. Tsimring, Continuum theory of partially fluidized granular flows, Phys. Rev. E 65 (2002) 061303.
[32] R. M. Nedderman, Statics and Kinematics of Granular Materials, Nova Science, 1991.
[33] A. Drescher, Analytical Methods in Bin-Load Analysis, Elsevier, 1991.
[34] P. A. Gremaud, J. V. Matthews, On the computation of steady hopper flows: I. stress determination for coulomb materials, J. Comput. Phys. 166 (2001) 63–83.
[35] P. A. Gremaud, J. V. Matthews, M. O'Malley, On the computation of steady hopper flows: Ii. von mises materials in various geometries, J. Comput. Phys. 200 (2004) 639–653.
[36] P. A. Gremaud, J. V. Matthews, D. G. Schaeffer, On the computation of steady hopper flows: Iii. model comparisons, J. Comput. Phys. 219 (2006) 443–454.
[37] M. L. Falk, J. S. Langer, Dynamics of viscoplastic deformation in amorphous solids, Phys. Rev. E 57 (1998) 7192–7205.
[38] A. Lemaître, Rearrangements and dilatency for sheared dense materials, Phys. Rev. Lett. 89 (2002) 195503.
[39] P. Jop, Y. Forterre, O. Pouliquen, A constitutive law for dense granular flows, Nature 441 (2006) 727–730.
[40] K. Kamrin, M. Z. Bazant, Stochastic flow rule for granular materials, Phys. Rev. E 75 (2007) 041301.
[41] K. Kamrin, C. H. Rycroft, M. Z. Bazant, The stochastic flow rule: A multi-scale model for granular plasticity, Modelling Simul. Mater. Sci. Eng. 15 (2007) S449–S464.
[42] J. Choi, A. Kudrolli, M. Z. Bazant, Velocity profile of gravity-driven dense granular flow, J. Phys.: Condensed Matter 17 (2005) S2533–S2548.
[43] J. Choi, Transport-limited aggregation and dense granular flow, Ph.D. thesis, Massachusetts Institute of Technology (2005).
[44] Z. Hashin, Analysis of composite materials— a survey., J. Appl. Mech.

50 (1983) 481.
[45] M. Ostoja-Starzewski, Scale effects in plasticity of random media: status and challenges, Int. J. Plasticity 21 (2005) 1119–1160.
[46] G. D. R. Midi, On dense granular flows, Euro. Phys. Journ. E. 14 (2004) 341–365.
[47] I. Goldhirsch, C. Goldenberg, On the microscopic fluctuations of elasticity, Euro. Phys. Journ. E 9 (2002) 245.
[48] http://lammps.sandia.gov/.
[49] P. A. Cundall, O. D. L. Strack, A discrete numerical model for granular assemblies, Geotechnique 29 (1979) 47.
[50] J. W. Landry, G. S. Grest, L. E. Silbert, S. J. Plimpton, Confined granular packings: structure, stress, and forces, Phys. Rev. E 67 (2003) 041303.
[51] L. E. Silbert, G. S. Grest, J. W. Landry, Statics of the contact network in frictional and frictionless granular packings, Phys. Rev. E 66 (2002) 061303.
[52] R. C. Brewster, J. W. Landry, G. S. Grest, A. J. Levine, Breakdown of bagnold scaling in cohesive granular flows, Phys. Rev. E 72 (2005) 061301.
[53] J. Christoffersen, M. M. Mehrabadi, S. Nemat-Nasser, A micromechanical description of granular material, J. Appl. Mech. 48 (1981) 339–344.
[54] W. Prager, D. C. Drucker, Soil mechanics and plastic analysis of limit design, Q. Appl. Mathematics 10 (2) (1952) 157.
[55] F. da Cruz, S. Emam, M. Prochnow, J. Roux, F. Chevoir, Rheophysics of dense granular materials: Discrete simulation of plane shear flows, Phys. Rev. E. 72 (2005) 021309.
[56] G. Lois, A. Lemaitre, J. M. Carlson, Numerical tests of constitutive laws for dense granular flows, Phys. Rev. E. 72 (2005) 051303.
[57] M. Depken, J. B. Lechman, M. van Hecke, W. van Saarloos, G. S. Grest, Stresses in smooth flows of dense granular media, Europhys. Lett. 78 (2007) 58001.
[58] A. J. M. Spencer, A theory of the kinematics of ideal soils under plane strain conditions, J. Mech. Physics 12 (1964) 337351.
[59] A. Schofield, C. Wroth, Critical State Soil Mechanics, McGraw-Hill, 1968.
[60] L. Anand, C. Gu, Granular materials: constitutive equations and strain localization, J. Mech. Phys. Solids 48 (2000) 1701–1733.
[61] J. W. Rudnicki, J. R. Rice, Conditions for the localization of deformation in pressure-sensitive and dilatant materials, J. Mech. Phys. Solids 23 (1975) 371.

Acknowledgments

This work was supported by the Director, Office of Science, Computational and Technology Research, U.S. Department of Energy under Contract Nos. DE-AC02-05CH11231 and DE-FG02-02ER25530; the National Science Foundation

under grants DMS-0410110 and DMS-070590; and also by the Norbert Weiner Research Fund and the NEC Fund at MIT.

Assessing continuum postulates in simulations of granular flow: supplementary figures

Chris H. Rycroft, Ken Kamrin, and Martin Z. Bazant

January 15, 2009

Description

This document contains additional plots of the stress and deformation rate tensors to supplement those in figure 4 of the paper. For each situation, the stress and deformation rate tensors are calculated in $5d \times 8d \times 5d$ boxes, using instantaneous information, with no time-averaging. The maximal stress eigenvector is shown purple, and the other two eigenvectors are shown in blue. The length of each component is proportional to the square root of the magnitude of the deviatoric stress eigenvalue. In the regions where deformation is occurring, the maximal and minimal eigenvectors of the deformation rate tensors are plotted in orange.

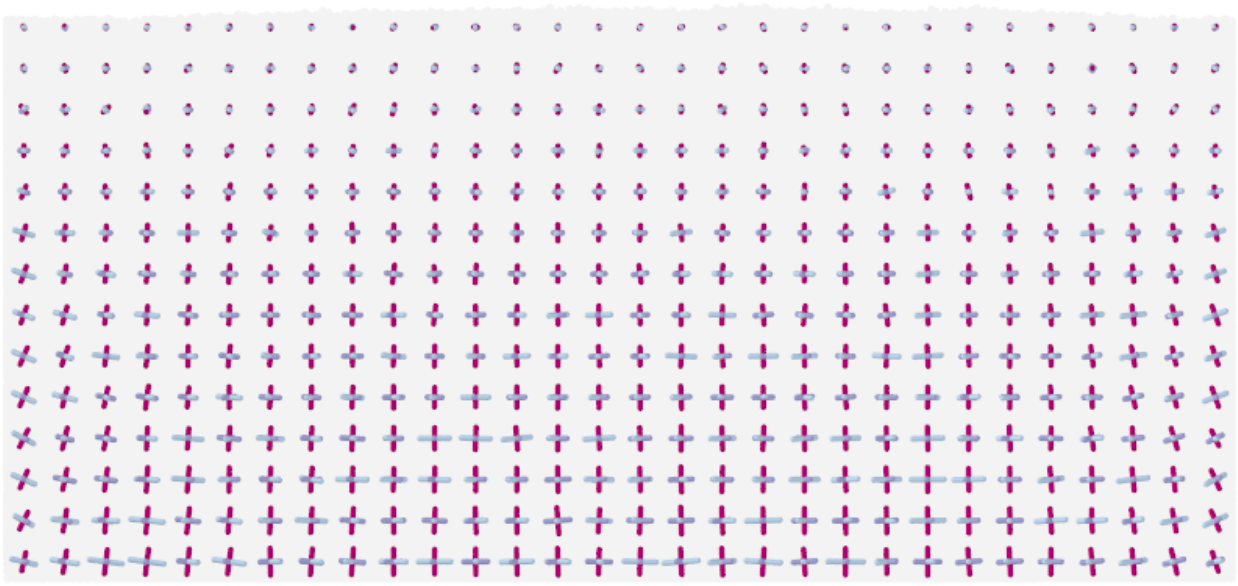

Figure S1: Plots of the directions and magnitudes of the eigenvectors of the deviatoric stress tensors for the wide initial packing.

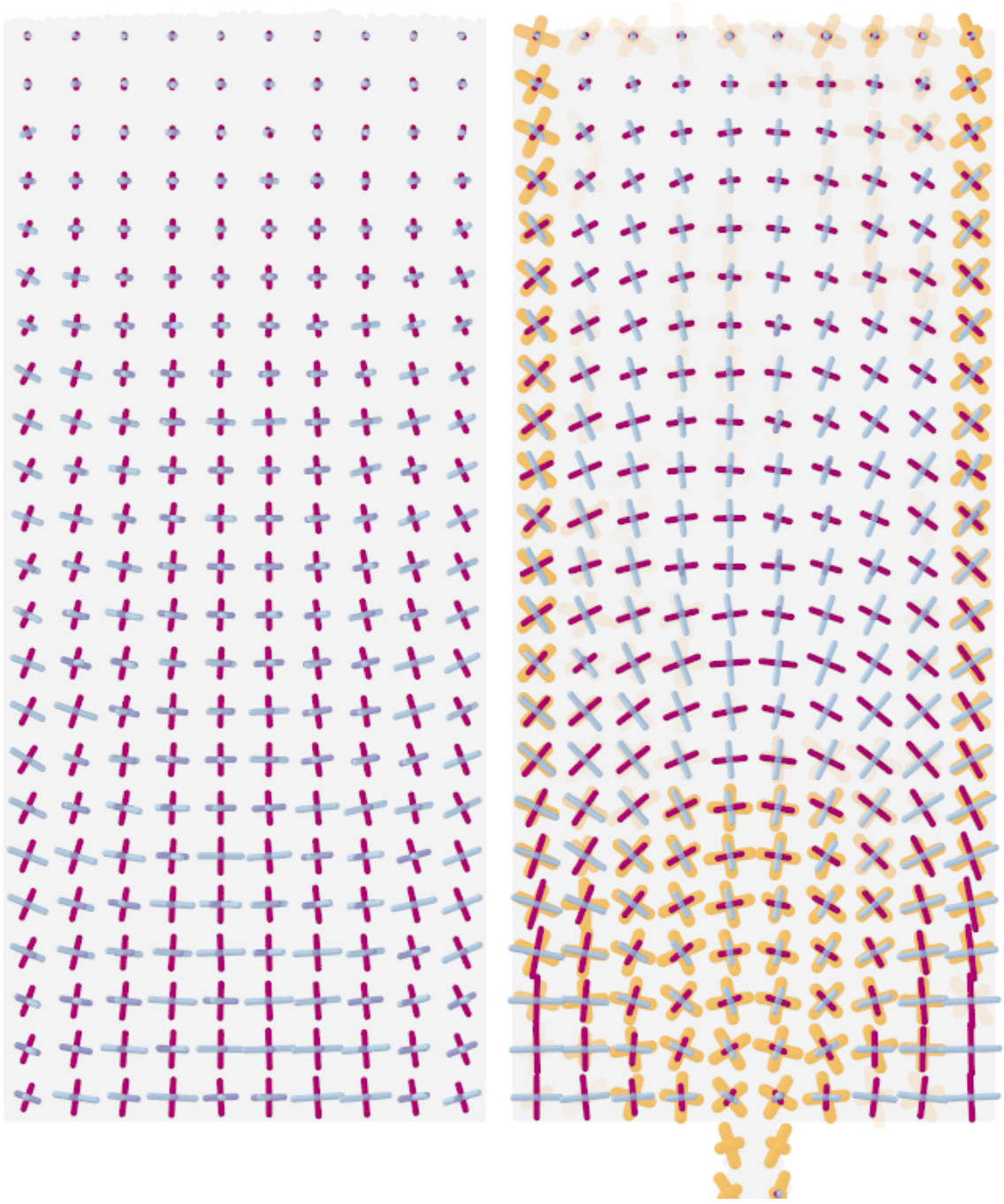

Figure S2: Plots of the directions and magnitudes of the eigenvectors of the deviatoric stress and deformation rate tensors for the tall silo before drainage (left), and during drainage (right). During drainage, a high degree of alignment between the two tensors can be seen.

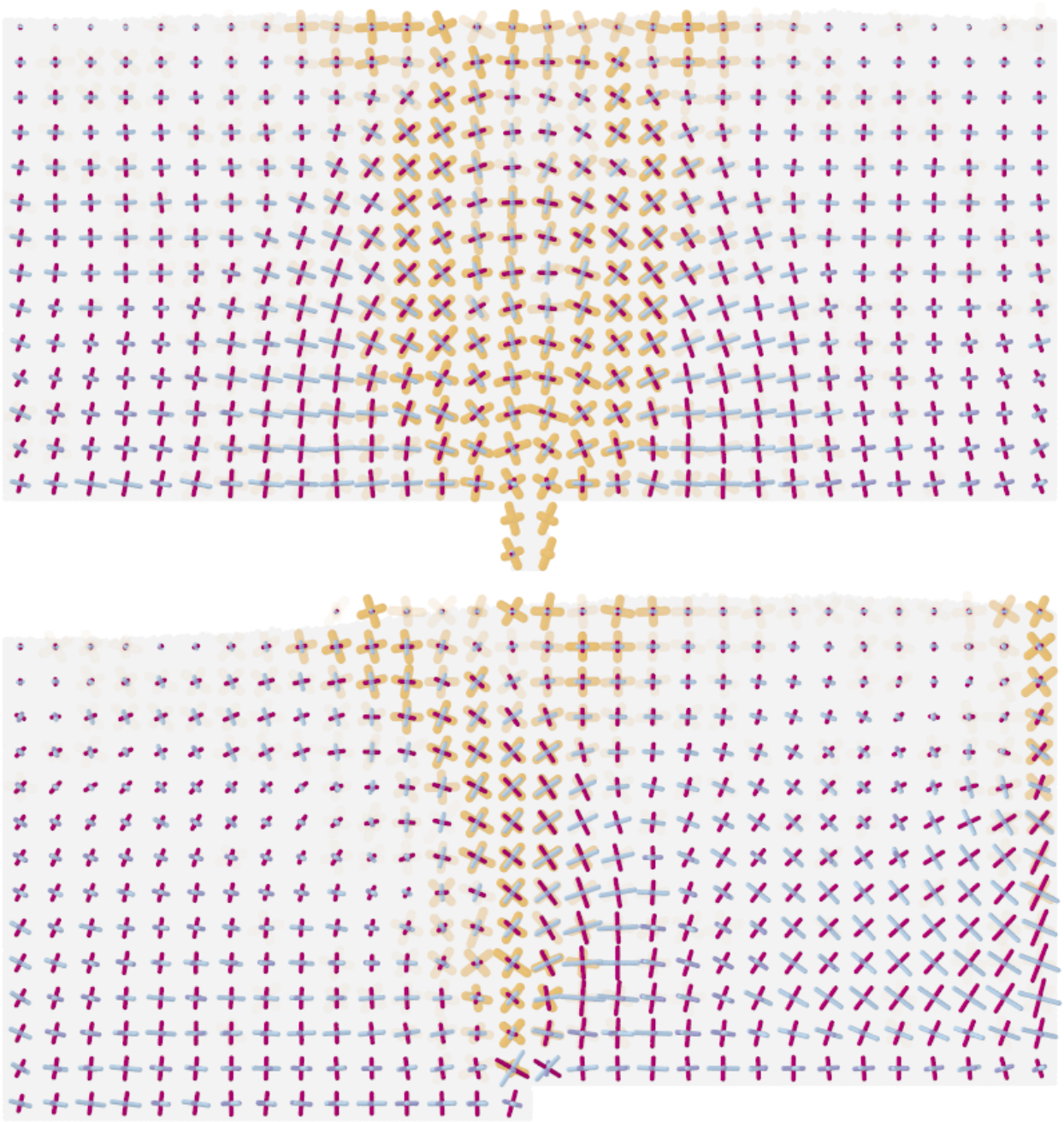

Figure S3: Plots of the directions and magnitudes of the eigenvectors of the deviatoric stress and deformation rate tensors for the wide granular packing during drainage (top), and during pushing (bottom). Again, a high degree of alignment between the two tensors can be seen.

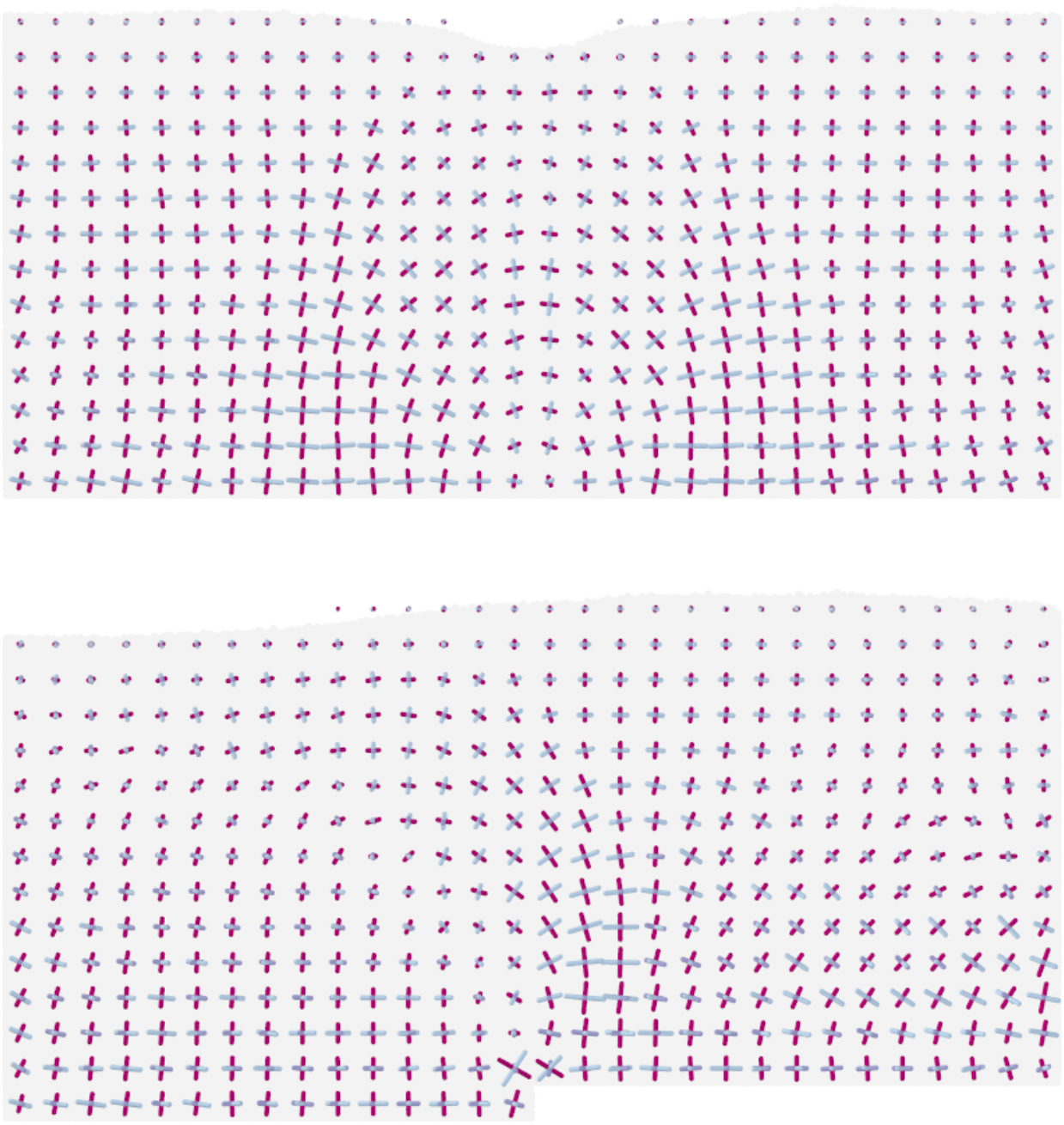

Figure S4: Plots of the directions and magnitudes of the eigenvectors of the deviatoric stress tensors after the drainage (top) and pushing processes (bottom) were arrested. The stress lines closely resemble those in the corresponding flowing states.